

# Supplemental Material for: Observation of a higher-order topological bound state in the continuum

Alexander Cerjan,\* Marius Jürgensen, Wladimir A. Benalcazar,† Sebabrata Mukherjee, and Mikael C. Rechtsman‡  
*Department of Physics, The Pennsylvania State University, University Park, Pennsylvania 16802, USA*

(Dated: October 13, 2020)

## I. EXPERIMENTAL FABRICATION AND SIMULATION PARAMETERS

We fabricated our waveguide arrays with a Yb-doped fiber laser (Menlo BlueCut) system emitting circularly polarized sub-picosecond (260 fs) pulse trains at 1030 nm with a repetition rate of 500 kHz. The light was focused inside a borosilicate glass (Corning Eagle XG) sample using an aspheric lens. The borosilicate glass sample was mounted on high-precision  $x$ - $y$ - $z$  translation stages (Aerotech). Each individual waveguide was written by translating the glass sample once through the focus of the laser at a speed of 10 mm/s. This process results in waveguides which only support the fundamental mode, which has an elliptical profile. However, by then orienting the lattice to be ‘diagonal’ with respect to the surface of the glass slide (i.e. the surface of the glass slide lies along the [1 1] direction of the lattice), the coupling constants between neighboring waveguides in both the [1 0] and [0 1] directions are the same, up to fabrication imperfections.

The waveguide arrays were measured using a commercial supercontinuum source (NKT SuperK COMPACT) with a filter to select the desired wavelength (SuperK SELECT). The beam was focused into the sample using an aspheric lens with an NA of 0.15 (ThorLabs C280TMD-B) and imaged onto the camera with an achromatic doublet (ThorLabs AC064-015-B-ML). The images were taken using a CMOS camera (ThorLabs DCC1545M).

Propagation within laser-written waveguide arrays can be modeled using the paraxial form of Maxwell’s equations,

$$i\partial_z\psi(\mathbf{r}, z) = \left[ -\frac{1}{2k_0}\nabla_{\mathbf{r}}^2 - \frac{k_0\Delta n(\mathbf{r})}{n_0} \right] \psi(\mathbf{r}, z). \quad (\text{S1})$$

Here,  $\psi(\mathbf{r}, z)$  is the amplitude of the slowly-varying envelope of the electric field,  $\mathbf{E}(\mathbf{r}, z) = \psi(\mathbf{r}, z)e^{(ik_0z - i\omega t)}\hat{\mathbf{e}}$ , and in which  $\hat{\mathbf{e}}$  is a unit vector denoting the polarization of the electric field, which lies in the transverse plane. As discussed in the main text,  $k_0 = \omega n_0/c$  corresponds to the propagation constant along the  $z$ -axis of the field in the absence of the waveguide, while  $\Delta n(\mathbf{r})$  is the spatially-dependent shift in the refractive index due to the laser inscription process, and  $\nabla_{\mathbf{r}}^2$  is the transverse Laplacian.

The effective coupling coefficient between neighboring waveguides can be calculated either through a modal overlap integral [1], or by finding the splitting between the eigenvalues of Eq. (S1) for a system with two waveguides. Again, note that the eigenvalues of Eq. (S1) physically correspond to shifts in the propagation constant,  $\beta = k_z - k_0$ , and that the coupling coefficients likewise correspond to coupling per unit length of propagation along the waveguides. Both of these methods require fixing the separation between the waveguides and the wavelength of the light (which enters into Eq. (S1) via  $k_0$ ), but for a fixed wavelength the coupling coefficient at different separations between the waveguides,  $l$  in the main text, is well approximated by  $t = A(\lambda)e^{-\alpha(\lambda)l}$ , where  $A(\lambda)$ ,  $\alpha(\lambda)$  are wavelength-dependent parameterizations, due to the exponential localization of the guided modes to each waveguide. For the experimental systems shown in the main text in Fig. 2, which are being operated at  $\lambda = 850$  nm,  $A = 733$  cm<sup>-1</sup> and  $\alpha = 0.47$  μm<sup>-1</sup>. These coupling coefficients can then be used to construct an effective tight-binding Hamiltonian for the system, which is what is written in Eq. 1 of the main text, or written in momentum space for an infinite waveguide array in Eq. 2 of the main text.

By experimentally measuring two-waveguide couplers and fitting to the observed coupling coefficients, we determined that the index shift of the waveguides can be modelled with a Gaussian profile,

$$\Delta n(\mathbf{r}) = \Delta n_0 e^{-r^2/\sigma_r^2} \quad (\text{S2})$$

with  $\Delta n_0 = 2.9 \cdot 10^{-3}$  and  $\sigma_r = 4$  μm. For a separation of 13 μm at  $\lambda = 850$  nm, this yields a tight-binding coupling coefficient of  $t = 1.62$  cm<sup>-1</sup>. For the waveguides used in breaking the chiral symmetry of the lattice as highlighted in

---

\* awc19@psu.edu

† wxb151@psu.edu

‡ mcrworld@psu.edu

Fig. 3 of the main text, the writing speed was incrementally decreased to be [8, 6, 4, 2] mm/s in Fig. 3e-h of the main text, respectively. These reduced writing speeds can be modeled numerically as shifts of the refractive index of the waveguides of  $\Delta n_0 = [3.1, 3.3, 3.5, 3.7] \cdot 10^{-3}$ .

## II. HIGHER ORDER BOUND STATE IN THE CONTINUUM WITHOUT SEPARABILITY

One known mechanism for creating bound states in the continuum (BICs) is through separability [2], in which the Hamiltonian of the system can be divided into two (or more) parts,

$$\hat{H}(\mathbf{r}) = \hat{H}_x(x) + \hat{H}_y(y) \quad (\text{S3})$$

that only depend on a single spatial coordinate. Then, by finding a localized bound state of each individual portion, for example,  $H_x(x)\psi_n(x) = E_n^{(x)}\psi_n(x)$  and  $H_y\phi_m(y) = E_m^{(y)}\phi_m(y)$ , the combined state,  $\psi_n\phi_m$ , is a bound state of  $\hat{H}(\mathbf{r})$  with energy  $E_n^{(x)} + E_m^{(y)}$ , which may reside within the continuum  $\hat{H}(\mathbf{r})$ . Furthermore, one may suspect that this is the origin of the BIC we report in the main text, as the tight-binding model corresponding to our waveguide arrays is separable.

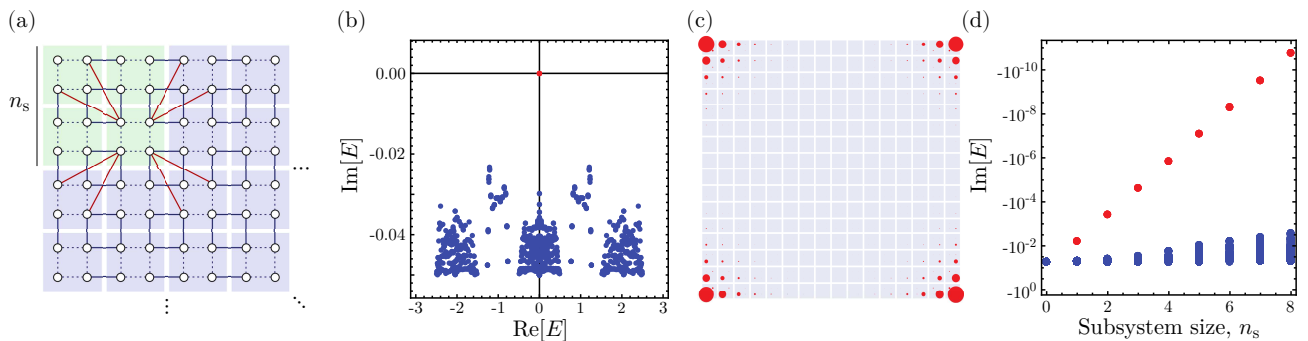


FIG. S1. (a) Schematic depicting the tight-binding model used as an example of a non-separable higher-order topological BIC. Dashed lines indicate couplings of  $t_{\text{intra}} = 0.25$ , solid black lines indicate couplings of  $t_{\text{inter}} = 1$ , and solid red lines indicate chiral-preserving non-separable couplings,  $t = 0.025$ . Only a single set of chiral-preserving non-separable couplings are shown for simplicity. Unit cells are indicated by shaded regions behind sets of nodes. Green unit cells are part of the ‘subsystem,’ while blue unit cells are part of the ‘environment,’ and have an added on-site loss of  $\gamma = 0.05$ . Only a single corner of the lattice is shown, but all four corners are part of the subsystem for these simulations, and do not have any on-site loss. (b) Eigenvalues for this lattice shown in the complex plane for  $n_s = 3$ , i.e. the total number of unit cells in each corner which constitute the ‘subsystem’ is  $3 \times 3$ . The lattice has  $n_1 = 16$  unit cells along its sides, for a total lattice size of  $16 \times 16$ . (c) The probability densities of the four eigenstates corresponding to the BICs from (b). (d) Plot of the decay rate of the eigenvalues of the lattice as  $n_s$  is increased.

However, this is not the origin of the protection of the BICs that we observe in our waveguide arrays [3]. To demonstrate this explicitly, in Fig. S1 we show numerical tight-binding calculations of a higher-order topological insulator that obeys both of the necessary protecting symmetries of the BIC,  $C_{4v}$  and chiral symmetry, but breaks separability. This lattice is schematically shown in Fig. S1a. We then divide this finite lattice into two regions, the ‘subsystem,’ a region of  $n_s$  unit cells next to each of the four corners of the lattice, and the ‘environment,’ which are the remainder of the unit cells in the lattice. A small, but non-zero, amount of loss is then added to the environment to simulate radiation loss,  $0 < \gamma \ll 1$ . As can be seen in Fig. S1b, this lattice still possesses four essentially real eigenvalues, whose corresponding eigenstates are exponentially localized to the corners of the lattice, see Fig. S1c. Finally, by changing the size of the device region, we can confirm that the energies of these corner-localized states exponentially converge to be real, confirming that these are BICs, not resonances, as shown in Fig. S1d.

Thus, even though the waveguide array that we study in the main text is separable, this separability is *not* what protects the BICs that we observe in our array. Even in the absence of separability, our arrays would still exhibit BICs, so long as the two necessary protecting symmetries,  $C_{4v}$  and chiral, were preserved.

## III. EFFECT OF NEXT-NEAREST-NEIGHBOR COUPLINGS IN THE WAVEGUIDE ARRAY

As discussed in the main text, in our waveguide arrays it is impossible to completely remove next-nearest-neighbor couplings between waveguides as the coupling strength is an exponentially decaying function of the spatial separation

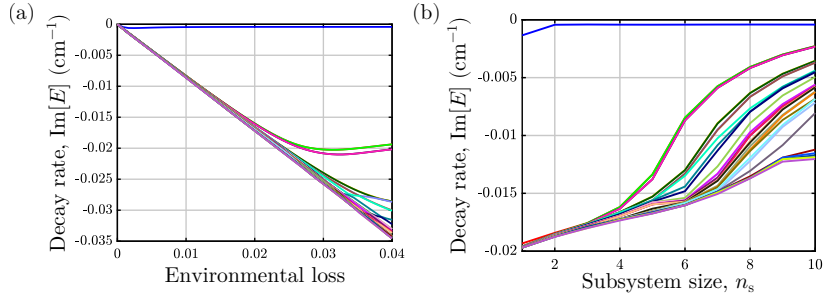


FIG. S2. (a) Plot of the decay rates of the 30 least lossy eigenvalues of the lattice as a function of the added loss,  $\gamma$ , to the waveguides in the environment. The plateau seen in the decay rate of the corner-localized mode corresponds to its true radiative rate in an infinite lattice. Here,  $n_l = 32$  (i.e. the total lattice size is  $32 \times 32$ ), and  $n_s = 4$ . (b) Plot of the decay rates of the 30 least lossy eigenvalues of the full lattice as a function of the edge length of the device region,  $n_s$  for  $\gamma = 0.02$  and  $n_l = 32$ . In both (a) and (b), the decay rate of the corner-localized mode is reaching a nearly constant value at approximately  $\text{Im}[E] = -4 \cdot 10^{-4} \text{cm}^{-1}$ .

between the waveguides,  $t(\lambda) = e^{-\alpha(\lambda)l}$ , in which  $\alpha(\lambda)$  is a wavelength-dependent constant. In particular, this means that the couplings between diagonally adjacent waveguides in our arrays will be non-vanishing, and break chiral symmetry, placing a practical limit on the decay length of the corner modes. However, in practice, the coupling coefficients corresponding to this process are small relative to the dominant energy scale in the array, i.e. the larger of  $t_{\text{intra}}$  or  $t_{\text{inter}}$  depending on whether the lattice is in the topological phase. For example, for the topological lattice shown in Fig. 2d,f of the main text,  $t_{\text{diag}}/t_{\text{inter}} \sim 0.08$ , where  $t_{\text{diag}}$  is the next-neighbor coupling strength between waveguides across the diagonal in the unit cell.

Moreover, we can calculate the effect of this coupling constant on the now-finite decay length of the corner-localized mode using a tight-binding model with a small amount of non-Hermitian loss added to an ‘environment’ region. Mathematically, this corresponds to

$$\hat{H}_{\text{tot}} = \hat{H} - \sum_{j \in \text{env. wgs.}} i\gamma |j\rangle\langle j|, \quad (\text{S4})$$

in which  $\hat{H}$  is given by Eq. 1 of the main text, and in which the sum runs over those waveguides in the environment. As can be seen in Fig. S2a, the decay length of the corner-localized mode quickly saturates as a function of the added loss to the environment, and this plateau corresponds to the radiative loss of the corner-localized resonance in an infinite lattice without added loss by the Limiting Absorption Principle [4–7]. Moreover, we can confirm this decay length of the corner-localized mode by fixing the added environmental loss and varying the size of the device region, shown in Fig. S2b. In both cases, the decay length converges to approximately  $\text{Im}[E] = -4 \cdot 10^{-4} \text{cm}^{-1}$ . As stated in the Main Text, for the topological lattice shown in Fig. 2d,f, the decay length is  $L_{\text{decay}} \sim 25 \text{m}$ , which is significantly longer than the waveguide arrays in our experiment ( $L = 7.6 \text{cm}$ ). As such, for the purposes of our experiment, our waveguide array is effectively chiral symmetric.

- 
- [1] H. A. Haus, *Waves and Fields in Optoelectronics* (Prentice Hall, Englewood Cliffs, NJ, 1983).
  - [2] C. W. Hsu, B. Zhen, A. D. Stone, J. D. Joannopoulos, and M. Soljačić, *Nature Reviews Materials* **1**, 16048 (2016).
  - [3] W. A. Benalcazar and A. Cerjan, *Phys. Rev. B* **101**, 161116 (2020).
  - [4] W. v. Ignatowsky, *Ann. Phys.* **323**, 495 (1905).
  - [5] D. M. Èidus, *Mat. Sb. (N.S.)* **57(99)**, 13 (1962).
  - [6] J. R. Schulenberger and C. H. Wilcox, *Arch. Rational Mech. Anal.* **41**, 46 (1971).
  - [7] A. Cerjan and A. D. Stone, *Phys. Scr.* **91**, 013003 (2016).